Journal of Colloid and Interface Science 463 (2016) 37–45

Contents lists available at ScienceDirect

Journal of Colloid and Interface Science

journal homepage: www.elsevier.com/locate/jcis

Toward a durable superhydrophobic aluminum surface by etching and ZnO nanoparticle deposition

Toktam Rezayi [a], Mohammad H. Entezari [a,b,*]

[a] Sonochemical Research Center, Department of Chemistry, Ferdowsi University of Mashhad, 91779 Mashhad, Iran
[b] Environmental Chemistry Research Center, Department of Chemistry, Ferdowsi University of Mashhad, 91779 Mashhad, Iran

GRAPHICAL ABSTRACT

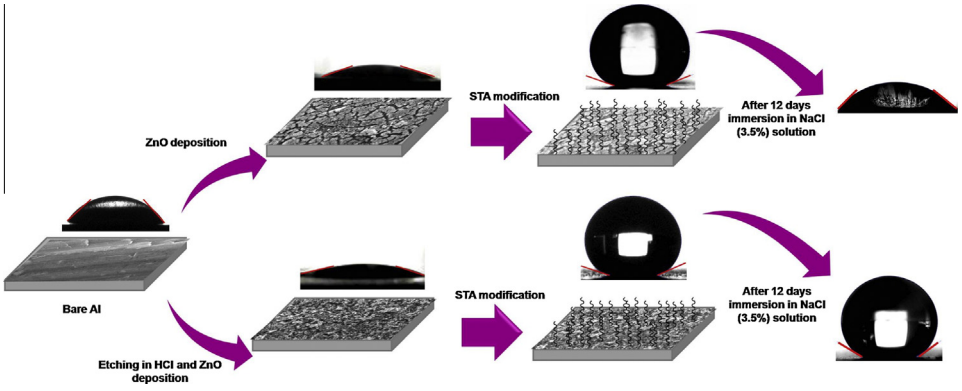

ARTICLE INFO

Article history:
Received 10 August 2015
Revised 11 October 2015
Accepted 13 October 2015
Available online 22 October 2015

Keywords:
Aluminum
Superhydrophobic surface
Ultrasound approach
ZnO deposition
Stearic acid
Etching

ABSTRACT

Fabrication of suitable roughness is a fundamental step for acquiring superhydrophobic surfaces. For this purpose, a deposition of ZnO nanoparticles on Al surface was carried out by simple immersion and ultrasound approaches. Then, surface energy reduction was performed using stearic acid (STA) ethanol solution for both methods. The results demonstrated that ultrasound would lead to more stable superhydrophobic Al surfaces (STA–ZnO–Al–U) in comparison with simple immersion method (STA–ZnO–Al–I). Besides, etching in HCl solution in another sample was carried out before ZnO deposition for acquiring more mechanically stable superhydrophobic surface. The potentiodynamic measurements demonstrate that etching in HCl solution under ultrasound leads to superhydrophobic surface (STA–ZnO–Al(E)–U). This sample shows remarkable decrease in corrosion current density (i_{corr}) and long-term stability improvement versus immersion in NaCl solution (3.5%) in comparison with the sample prepared without etching (STA–ZnO–Al–U).

Scanning electron micrograph (SEM) and energy-dispersive X-ray spectroscopy (EDX) confirmed a more condense and further particle deposition on Al substrate when ultrasound was applied in the system. The crystallite evaluation of deposited ZnO nanoparticles was carried out using X-ray diffractometer (XRD). Finally, for STA grafting verification on Al surface, Fourier transform infrared in conjunction with attenuated total reflection (FTIR–ATR) was used as a proper technique.

* Corresponding author at: Sonochemical Research Center, Environmental Chemistry Research Center, Department of Chemistry, Ferdowsi University of Mashhad, 91779 Mashhad, Iran.
E-mail addresses: entezari@um.ac.ir, moh_entezari@yahoo.com (M.H. Entezari).

http://dx.doi.org/10.1016/j.jcis.2015.10.029
0021-9797/

1. Introduction

Water repellency and self-cleaning properties are the most important characteristics of the lotus leaves. These observable characteristics are common in natural world. For example, the butterfly's wings are coated with special shapes that give unique morphology to wing surface and lead to superhydrophobic characteristic [1]. In superhydrophobic surfaces, the water contact angle (WCA) is upper than 150° and the sliding angle (SA) is lower than 10°. The study of natural superhydrophobic substrate pointers to this fact that roughness of surface and reduction of surface tension are principle factors in superhydrophobic properties [2–6]. For creation a rough surface, different methods such as sol-gel, chemical deposition and electro deposition have been utilized. After acquiring a proper roughness, surface energy reduction can be done using fatty acids [7–9]. Recently, these surfaces have attracted much attention because of employing in drag reduction of underwater container, corrosion resistance of metals and water repellency [10–12].

Al and its alloys possess advanced mechanical and physical characteristics such as high plasticity, easy processing and low density; therefore their widely use can be observed in automotive, aviation, aerospace and so on [13]. Moreover, Al and other metals have high surface energy and consequently are faced with a number of contamination problems [14]. As a result, superhydrophobic metals, which keep away water droplet, have significant application in avoiding the corrosion and polluting by wastewater [14].

There are numerous attempts for superhydrophobic Al fabrication. For example, Wu and Zhang obtained superhydrophobic Al using electrochemical method and modification of rough surface with fluorine silane [15]. In another work, Guo and Wang employed simple immersion method and surface energy reduction with stearic acid (STA) for superhydrophobic Al creation [16]. Furthermore, Song and Xu have conducted a simple immersion method and subsequently surface energy reduction in order to acquiring superhydrophobic Al substrate [8].

In current work, for having a desirable roughness, ZnO particle deposition has been performed using simple immersion and ultrasound methods. There is not any report on using ultrasound for particle deposition on Al substrate for having a superhydrophobic surface. Therefore, the novelty of this work is the use of ultrasound in fabrication of Al superhydrophobic surfaces. Ultrasound can create unique conditions that induce different changes. The changes are resulted from cavitation phenomena, which is composed of three steps: formation, growth and suddenly implosive collapse of bubbles in liquid. The cavitation can produce local hot spots with a temperature of nearly 5000 °C and pressure of about 500 atmospheres [17]. In heterogeneous environment, the collapse of bubble is asymmetric and affects the surface morphology through the creation of micro-jets and shock waves. It is expected that distinct topography has dramatic influence on the surface wettability and stability of the resulted superhydrophobic surfaces. This expectation has been satisfied completely in this work and ultrasound showed a critical role in particle deposition to reach a more stable superhydrophobic surface. Additionally, etching in HCl solution before ZnO particle deposition led to a hierarchical roughness, which enhanced the superhydrophobic stability. Finally, the corrosion resistance of superhydrophobic surfaces has been examined using potentiodynamic polarization measurements.

2. Experimental

2.1. Material

Commercial pure aluminum in dimensions of 20 mm × 15 mm × 4 mm were utilized for this work. Zinc acetate dihydrate ($Zn(AC)_2{\cdot}2H_2O$, 98%, Riedel), thriethylamine (TEA, 99%, Merck), ethanol (96%, Riedel), hydrogen chloride (HCl, 37%, Merck), stearic acid (STA, 99%, BDH), sodium chloride (NaCl, 99.5%, Merck) and distilled water were used as received.

2.2. Fabrication of superhydrophobic Al

In outset, Al plates have been polished with sand paper (1500 mesh), washed with ethanol and distilled water carefully to remove any pollutant. After that, the cleaned Al substrates were immersed into 50 mL aqueous solution containing $Zn(AC)_2$ (0.01 M) and thriethylamine (0.1 M) and stirred for various interval times at 40 °C. Al plates were withdrawn carefully from the solution, washed with distilled water and dried at 100 °C for 1 h. The as-prepared ZnO-deposited Al substrate was modified by STA ethanol solution with various concentration and for a range of immersion time. Al substrates were withdrawn from STA solution, washed thoroughly with ethanol and dried at 80 °C for 10 min. This step resulted in Al surfaces with high WCA and low SA values. It should be mentioned that the WCA and SA measurements have been performed on the samples after reaching to ambient temperature.

In ultrasonic method, ultrasound has been employed instead of stirring for a wide range of sonication time and acoustic amplitude. Modification with STA ethanol solution was conducted at optimal condition obtained from simple immersion (classic) way.

2.3. Superhydrophobic Al with enhanced stability

For obtaining more stable superhydrophobic surface, the cleaned Al substrate was immersed in HCl (10%) solution for 10 min. After washing and drying of etched Al, ZnO particle deposition was carried out using ultrasonic method for different time durations. Finally, the reduction of free surface energy was completed using STA ethanol solution (STA–ZnO–Al(E)–U). In Table 1, different samples names are summarized based on the synthesis processing.

Table 1
Symbols for different samples prepared using various routs.

Sample symbol	Descriptive of the sample
B. Al	Bare Al with the polishing processing
ZnO–Al–I	ZnO nanoparticles were deposited using simple immersion (classic) method at optimized conditions
ZnO–Al–U	ZnO nanoparticles were deposited using ultrasound method at optimized conditions
Al(E)	Al has been etched in HCl (10%) for 10 min
ZnO–Al(E)–U	ZnO nanoparticle deposition by ultrasound was carried out at optimized conditions after etching of Al in HCl solution
STA–B. Al	Bare Al was modified with STA at optimized concentration and time immersion
STA–Al(E)	Etched Al was modified with STA at optimized concentration and time immersion
STA–ZnO–Al–I	ZnO–Al–I was modified with STA at optimized concentration and time immersion
STA–ZnO–Al–U	ZnO–Al–U was modified with STA at optimized concentration and time immersion
STA–ZnO–Al(E)–U	ZnO–Al(E)–U was modified with STA at optimized concentration and time immersion

2.4. Characterization

The crystallite structure of samples was measured using X-ray diffraction (XRD) analysis on a PANalytical X'Pert Pro MPD X-ray diffractometer supplied with Ni-filtered Cu Kα radiation (λ = 1.54178 Å). The tube voltage was 40 kV with a tube current of 40 mA. The 2θ angular areas between 30° and 70° were explored at a scan rate of 0.026° min^{-1}. The chemical composition of samples was illustrated using an energy-dispersive X-ray spectroscope (EDX, INCA 7353, England) and an attenuated total reflection in conjunction with Fourier-transform infrared spectrophotometry (ATR–FTIR, Shimadzu-IR-460 spectrometer). In ATR–FTIR analysis, ZnSe crystal with refraction index of 2.4 was employed. The sample was held in contact with crystal and the IR rays were made incident on the sample at angle of 45°. The light that was entirely reflected by the boundary between the sample and the crystal was measured to achieve an infrared spectrum. Besides, all the Shimadzu FTIR series spectrophotometers are single-beam type. The surface morphology was characterized using a scanning electron microscope (SEM, LEO 1450 VP, Germany).

2.5. Contact angle and sliding angle measurements

For WCA measurement, a homemade apparatus has been used. 10 µl water droplets were dropped carefully onto the surface of substrates. The usual droplet size utilized in WCA assessment is in the range of 1–10 µl. Once the droplet volume rises, the gravity becomes greater. Thus, droplets larger than 10 µl are not normally applied. With a camera (Canon SX200, Japan), water droplets images were captured and then were examined using MATLAB software for acquiring WCA. A simple device has been designed for SA measurements. This tool possesses a mutable plane for oriented Al substrate until water droplet start to roll off. Since, the maximum position for the movable plane is 90°, the highest reported SA is equal to 90°.

2.6. Mechanical stability measurements

The abrasion test was carried out in order to examine the mechanical stability of the resulted superhydrophobic surfaces. The surface was placed on the abrasive film (1500 mesh), and pulled in one direction with speed of 10 mm/s at a stroke of 25.50 cm. In addition, the weight equals to 300 g was applied to the specimen (Fig. S1). The variation of WCA values after each abrasion test cycle was recorded.

2.7. Electrochemical measurements

A standard three-electrode cell was used as working cell. In this cell, Pt and Na Ag/AgCl have been selected as counter and reference electrodes, respectively. The specimen was considered as working electrode. This electrode has area of 1 cm^2. All tests were carried out at room temperature (20 °C) in aqueous solution of sodium chloride (NaCl, 3.5%). All specimens were immersed in NaCl solution for 1 h to reach the stable state before potentiodynamic polarization test. Furthermore, the scanning of potential was performed from −200 to −1000 mV at a scan rate of 2 mV s^{-1}.

3. Results and discussion

3.1. WCA and SA for the sample prepared in classical method

WCA as well as SA results for the sample prepared in classic approach have been represented in Fig. S2. According to this figure, with increasing the immersion time in $Zn(AC)_2$–TEA solution, WCA increased and reached a plateau at 15 min. The SA falls to the lowest level at this point too. Further immersion in $Zn(AC)_2$–TEA solution has not dramatic effect on SA and WCA. It must be noted that, these results have been obtained after STA modification in STA ethanol solution with concentration of 0.014 M for 1 h.

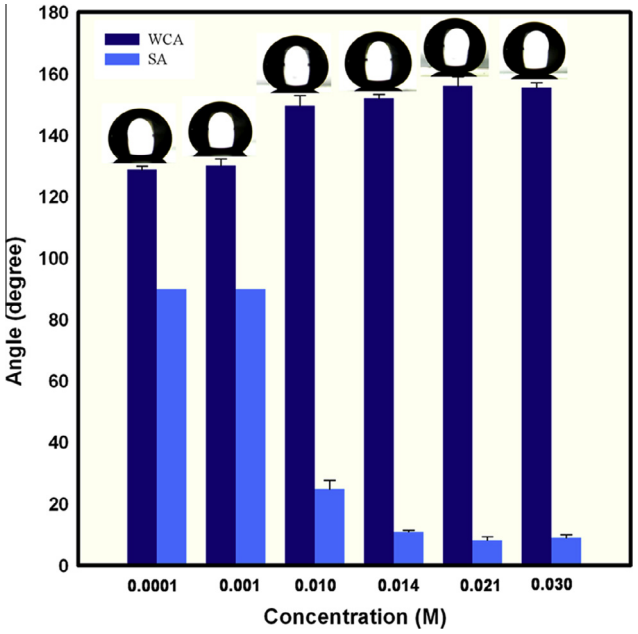

Fig. 1. WCA and SA versus different STA concentrations.

Therefore, immersion in $Zn(AC)_2$–TEA solution for 15 min has been selected as optimal time. Also, the influence of STA concentration and immersion time in this solution must be investigated. The results of this assessment have been shown in Figs. 1 and S3. Fig. 1 shows WCA and SA for Al surfaces deposited with ZnO during immersion in $Zn(AC)_2$–TEA solution for 15 min and modified with STA ethanol solution in a wide range of concentration for 1 h.

Undoubtedly, according to Fig. 1 it can be inferred that WCA values increase gradually with STA concentration upsurge. Moreover, the SA data demonstrate a reduction with STA concentration growth. The highest WCA (156.16° ± 2.89°) and the lowest SA (8.30° ± 1.20°) have been concluded with STA solution of 0.021 M.

Fig. S3 explains WCA for ZnO-deposited Al surfaces through immersion in $Zn(AC)_2$–TEA solution for 15 min and modified with 0.021 M STA ethanol solution for different modification times. Based on this figure, WCA reaches to 153.16° ± 1.83° after immersion for 10 min. The SA value is not sufficient small to give

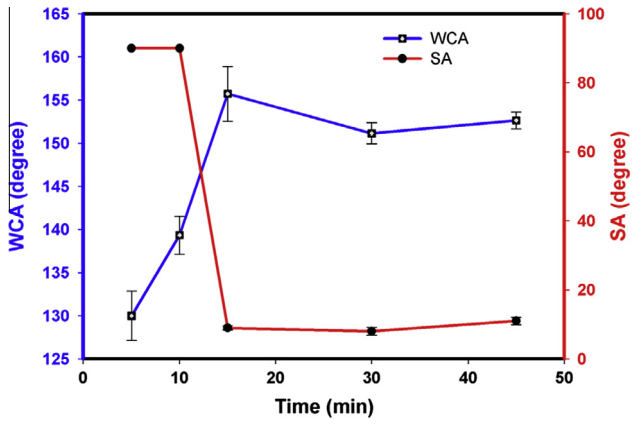

Fig. 2. WCA and SA versus sonication time.

low adhesive superhydrophobic surface (40.00° ± 2.88°). Immersion for 1 h leads to maximum WCA and low SA values (8.30° ± 1.20°) and is a suitable modification time. Further immersion time has minor effect on WCA and SA. Therefore, 1 h immersion time has been considered as optimum value.

3.2. WCA and SA for the sample prepared in ultrasonic method

In this case, it is essential to optimize the important characteristics of ultrasonic wave such as sonication time and acoustic amplitude. Fig. 2 shows WCA and SA data for ZnO-deposited Al surfaces resulted by immersion in $Zn(AC)_2$–TEA solution under different interval times of sonication. Furthermore, all substrates were modified with 0.021 M STA ethanol solution for 1 h. In addition, the amplitude of acoustic waves has been fixed at 30%. As can be seen in Fig. 2, when sonication time reaches to 15 min, the WCA is at highest level of 155.72° ± 3.19°. The value of SA at this point is equal to 9.00° ± 0.57° which is enough small to conclude low adhesive property for superhydrophobic Al. Therefore, 15 min of sonication time has been selected as an appropriate optimized time.

Moreover, by applying ultrasound, it is necessary to optimize the amplitude of acoustic waves. The results of this assessment have been demonstrated in Fig. S4. For this purpose, four different levels of amplitude (20%, 30%, 40%, and 50%) have been studied. In all cases, sonication time is 15 min, STA concentration, and immersion time in modifier solution are equal to 0.021 M and 1 h, respectively.

The WCA is 151.67° ± 3.16°, 155.72° ± 3.19°, 163.78° ± 1.47°, and 156.30° ± 3.16° when amplitude is 20%, 30%, 40%, and 50% correspondingly. Therefore, for ultrasound method with amplitude of 40%, the highest value of WCA will be resulted. Besides, the SA at this point is very low (2.33° ± 0.88°). As a result, for ultrasound approach, the optimized sonication time and amplitude have been regarded as 15 min and 40%, respectively.

Based on the obtained results, both classic and ultrasound methods are able to acquire superhydrophobic property on Al substrate. Although, the highest WCA concluded by ultrasound technique 163.78° ± 1.47° is more than of corresponding value resulted by classic ones (156.16° ± 2.89°).

3.3. Superhydrophobic stability against immersion in water

Another important factor is stability of acquired superhydrophobic surfaces against immersion in distilled water. This trend has been evaluated for superhydrophobic Al resulted by classic and ultrasound methods at their optimized conditions.

According to Fig. 3, when ultrasound was used for ZnO particle deposition, WCA is 163.78° ± 1.47° and after immersion in water

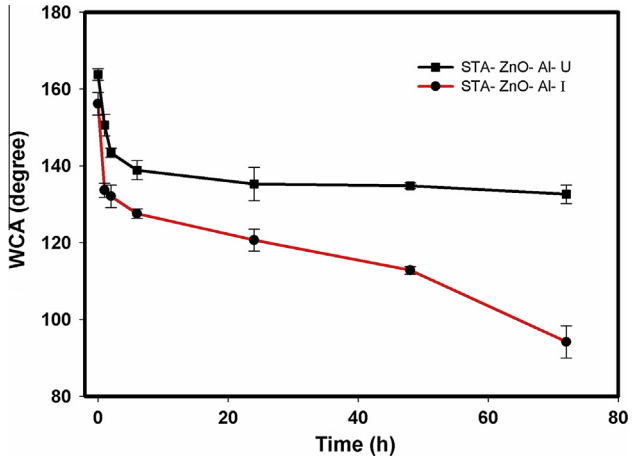

Fig. 3. WCA of STA–ZnO–Al–U and STA–ZnO–Al–I versus immersion time in water.

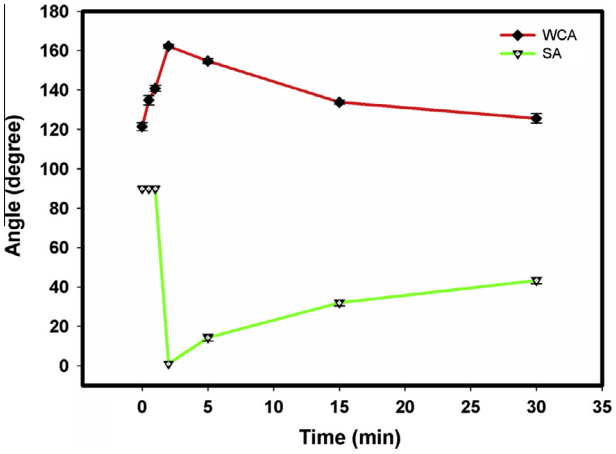

Fig. 4. WCA and SA versus time of sonication in $Zn(AC)_2$–TEA solution.

for three days, this value reduces to 132.60° ± 2.39°. For classic approach, WCA is 156.16° ± 2.89° and after immersion in water for three days, this value falls to 94.17° ± 4.17°. Therefore, more stable superhydrophobic surface can be created using ultrasound. However, this stability is not sufficient for practical application.

3.4. Superhydrophobic surfaces with high stability

Creation of hierarchical roughness with two-scale unevenness can be helpful for stability enhancement. Etching of Al in HCl (10%) for 10 min and subsequently ZnO particle deposition with effective ultrasound method can improve stability of superhydrophobic surfaces. This deposition is carried out in a variable range of ultrasound irradiation time in $Zn(AC)_2$–EDA solution. The amplitude of acoustic waves has been maintained at 40%. Besides, all surfaces have been modified with 0.021 M STA ethanol solution for 1 h before WCA measurement.

From Fig. 4, it can be pointed out that, before ZnO particle deposition, WCA is 121.41° ± 2.01°. After sonication in $Zn(AC)_2$–TEA solution, WCA climb dramatically, reaching the highest point of 162.17° ± 0.93° 2 min. Further increase in sonication time leads to considerable slump in WCA results. For more investigation, the stability of resulted superhydrophobic surface versus immersion time in water is examined. The results of this measurement are presented in Table S1.

In this case, high WCA values maintain over 360 h immersions in water. Moreover, comparison between mechanical stability of superhydrophobic surfaces has been demonstrated in Fig. S5. It should be noted that, ultrasound approach has been used for ZnO particle deposition and WCA values have been reported after STA modification. It is clear from Fig. S5 that more mechanical durable superhydrophobic surface is resulted when etching in HCl is carried out before ZnO nano particle deposition. Consequently, creation of hierarchical roughness is a practical way to improve the stability of superhydrophobic characteristic. For assessment the reason of observed phenomena, identification techniques have been employed. In all cases, the investigated surface has been resulted at optimal conditions.

4. Analysis

4.1. SEM and EDX assessment

4.1.1. ZnO–Al–I and ZnO–Al–U

The surface morphologies of polished and ZnO-deposited Al substrates using classic and ultrasound methods (ZnO–Al–I and

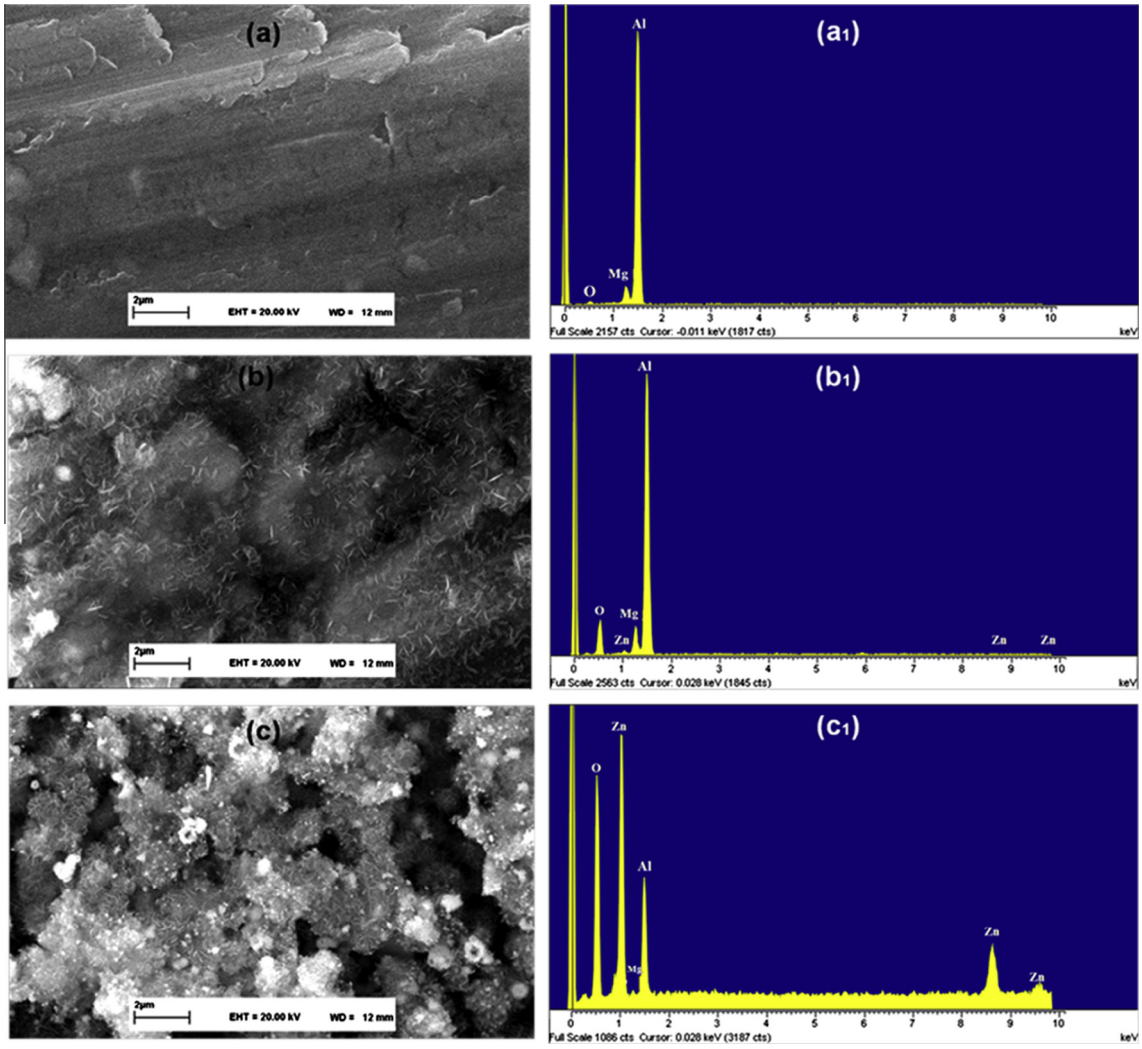

Fig. 5. SEM images (left) and EDX spectra (right) of B. Al (a and a_1), ZnO–Al–I (b and b_1) and ZnO–Al–U (c and c_1) methods.

ZnO–Al–U) are demonstrated in Fig. 5. According to Fig. 5a, polished Al possesses a smooth surface. Nevertheless, there are several scratches created by the polishing processing. After ZnO deposition using classic method (Fig. 5b), the surface seems nearly flat and exact observation reveals the presence of nanostructures distributions on Al substrate. The roughness, which is created with this morphology, can lead to superhydrophobicity after surface energy reduction. However, this one-scale unevenness is not in favor of stable superhydrophobic surface. Low density of nanostructures can lead to penetrate of water droplet molecules to pits and consequently WCA decreased considerably after immersion in distilled water.

Using ultrasonic approach for particle deposition, different morphology concluded in comparison with classical one. According to Fig. 5c, there are condense and uniform microstructures on Al surface. A number of these microstructures are formed huge particles, but others are disconnected and form voids.

The observed difference morphology of deposited ZnO nanoparticles can be attributed to unique conditions induced by ultrasound. In heterogeneous system, the strong streams (shock waves and microjects) created by asymmetric collapse are responsible for effective collisions between particles [18]. As a result, more particle fusion and as well as further agglomeration of ZnO particles can be occurred on the surface. In this case, more air pockets entrap between holes and water molecules penetrate with delay in comparison with classical method. The trend of superhydrophobic stability as a function of time immersion in distilled water (Fig. 3) can be interpreted base on these illustrations.

Additionally, EDX spectra as a helpful technique can demonstrate the existence of available elements on Al substrate. Firstly, it must be noted that Mg is present in Al alloys and can be observed in EDX spectra. Based on Fig. 5a_1 only Al, Mg and slight O elements are detected in polished Al surface. For ZnO-deposited Al surface using classic method, the emergence of Zn peak and intensify of O peak can be a reason for ZnO deposition on Al substrate. Further study of these spectra can demonstrate a very outstanding difference between ZnO-deposited Al surface spectra using classic and ultrasound methods. It is obvious from Fig. 5c_1 that Zn and O spectra are very intense when ultrasound is used for particle deposition. In contrary, the intensity of Al and Mg spectra becomes weaker and EDX results confirm more deposition of ZnO particle on Al surface associated with ultrasound method instead of classical one. These results are extremely compatible with SEM images.

4.1.2. Al(E) and ZnO–Al(E)–U

Al etching in HCl leads to numerous rectangle-shape pits and protrusions on the surface (Fig. 6a). The surface roughness with large pores (2–10 μm) does not lead to superhydrophobicity after STA modification (Fig. S6). By ZnO particle deposition on etched Al under ultrasound for 2 min, the surface acquires combination

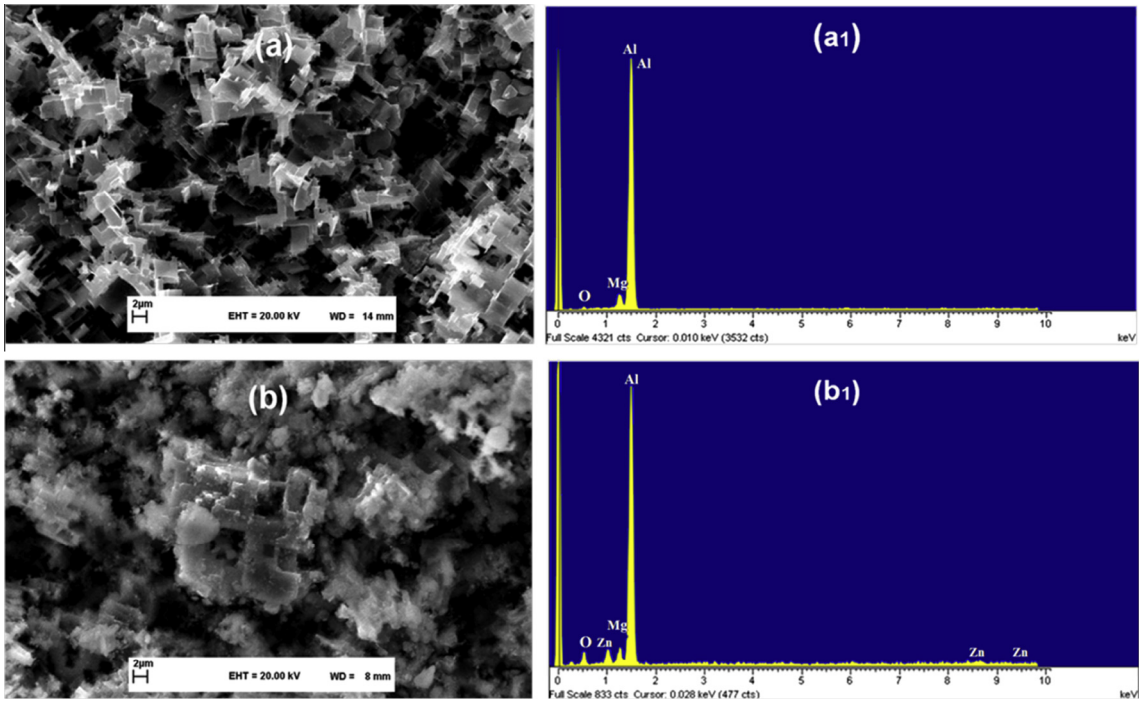

Fig. 6. SEM images (left) and EDX spectra (right) of Al(E) (a and a_1) and ZnO–Al(E)–U (b and b_1).

morphology with a range of hierarchy, microstructures, and submicro and nano ZnO particles. Such hierarchical structure is in favor of improved stability. The elemental analysis of corresponding surfaces has been represented in Fig. 6a_1 and b_1.

Based on Fig. S6B, Al is hydrophilic and after STA modification, WCA increases from 50° to roughly 95°. Therefore, STA modification is not sufficient for giving a superhydrophobic property to the Al surface. Al etching in HCl creates numerous pits and peaks on the surface, air can be trapped after STA modification, and WCA increases to 121.41°. However, due to wide voids and pits on this surface, air cannot be trapped effectively to yield superhydrophobic state after STA modification. Deposition of ZnO for 2 min on etched Al surface leads to filling the wide valley by ZnO nanoparticles. Therefore, the size of voids reduces to appropriate value for air trapping. However, further ZnO particle deposition may fill completely the pits and subsequently surface roughness and WCA can be decreased (Fig. 4).

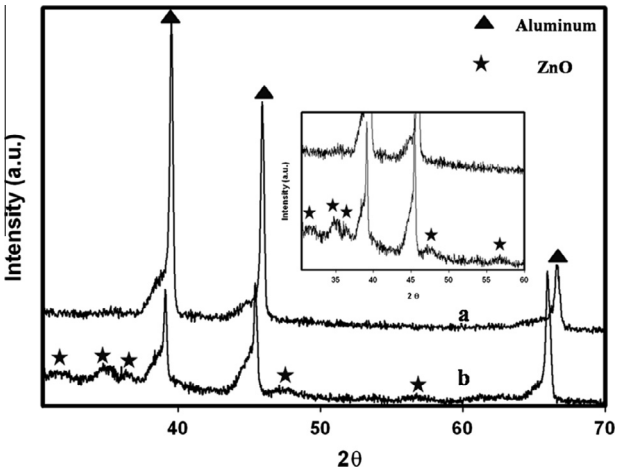

Fig. 7. XRD spectra of (a) ZnO–Al–I and (b) ZnO–Al–U.

4.2. XRD assessment

The XRD patterns of ZnO-deposited Al surface with both classic and ultrasound methods have been demonstrated in Fig. 7. It is clear that for classic method only characteristic peak of Al is distinguishable. However, for ultrasound method, extra peaks are observed which can be assigned to ZnO particles.

According to Fig. 7a for classic technique, the peaks appeared at 2θ = 39.49, 45.88, and 66.58 are related to Al substrate [19]. Additionally, there is not any extra peak in this pattern. As presented previously, less ZnO particle deposition on Al substrate using classic method was proved using SEM and EDX results. Consequently, it was expectable that XRD analysis cannot verify the existence of ZnO particles. However, using ultrasound for ZnO particle deposition, different XRD pattern has been created (Fig. 7b). There are several peaks, which are corresponding to hexagonal ZnO [19]. In addition, these peaks are broad and weak that can be a sign of weak crystallinity of deposited particles. Furthermore, the shift of Al characteristic peak to smaller angle after ZnO deposition indicates the increase of lattice parameters [20].

4.3. ATR–FTIR analysis

ATR–FTIR technique is highly recommended for chemical composition assessment. The corresponding spectra of B. Al, ZnO–Al–U, ZnO–Al(E)–U, and STA–ZnO–Al(E)–U surfaces have been demonstrated in Fig. 8. Based on Fig. 8, for B. Al, only one weak distinguishable peak is appeared at 460 cm^{-1} which is characteristic peak of Al–O bond [21]. For ZnO–Al–U surface, the appearance of intense peak at 416 cm^{-1} is assigned to wurtzite ZnO [22]. Furthermore, the emergence of two peaks at 447 cm^{-1} and 550 cm^{-1} can be assigned to ZnO stretching [23,24]. Additionally, another two peaks which are located about 750 cm^{-1} and 1360 cm^{-1}, can be correlated to Zn–O bond [25–28]. As an IR pattern is a plot of transmittance percent versus wavenumber, the energies of bond

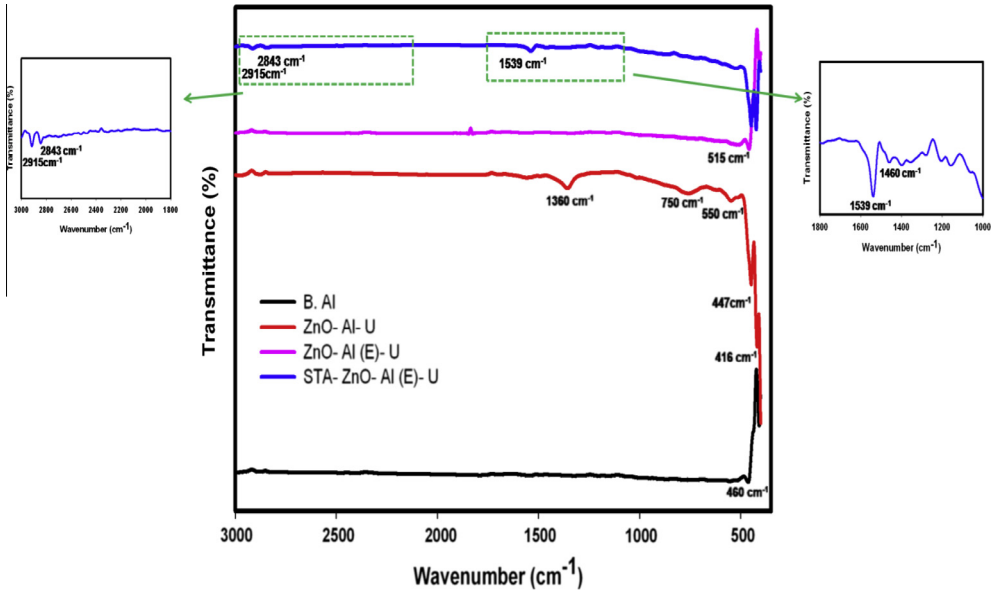

Fig. 8. ATR–FTIR spectra of different substrates.

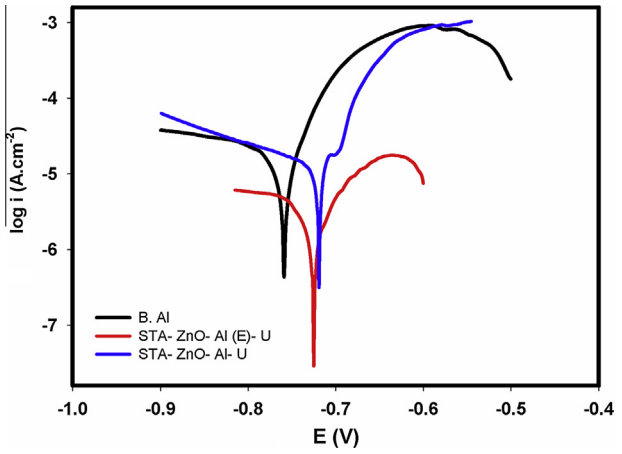

Fig. 9. Potentiodynamic polarization curves of B. Al, STA–ZnO–Al–U and STA–ZnO–Al(E)–U substrates.

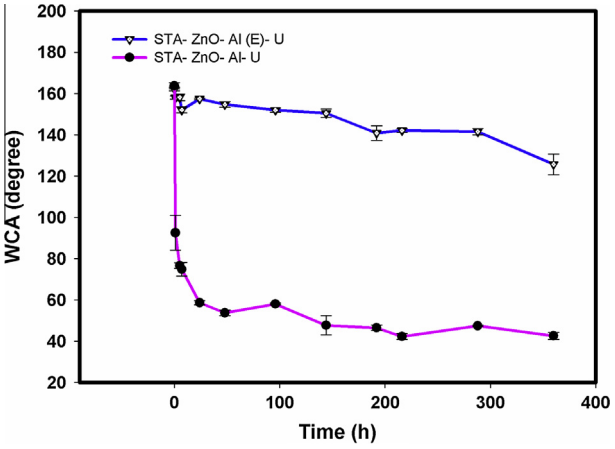

Fig. 10. Long-term stability of STA–ZnO–Al–U and STA–ZnO–Al(E)–U in NaCl solution (3.5%).

vibration vary with movement on the graph in horizontal direction. As a result, the horizontal location of the absorption band relates to dissimilar energy. Two factors, which are crucial in stretching energy determination, are masses of bonded atoms and bond strength. Therefore the emergence of ZnO bond at higher wavenumber (1360 cm^{-1}) can be assigned to its higher strength [29]. For ZnO–Al(E)–U surface, the presence of a peak at 515 cm^{-1} is attributed to the vibration modes of ZnO [30]. Consequently, FTIR–ATR is supportive technique for ZnO deposition proof.

In another hand, the grafting of STA can be clearly approved according to Fig. 8. For STA–ZnO–Al(E)–U, the peaks which are visible at 2843 cm^{-1} and 2915 cm^{-1} are assigned to υCH_2 and υCH_3, respectively. These peaks can be a sign of a long-chain alkyl group existence on the surface [31]. Moreover, two new peaks are appeared at 1460 cm^{-1} and 1539 cm^{-1} that are resulted from symmetric and asymmetric stretches of RCO_2^- group [31]. According to the dissimilarity between symmetric and asymmetric peaks of RCO_2^-, the coordination between zinc ion and stearate ion can be inferred to the bi-dentate form. Zinc stearate molecules contain of a long non-polar chain having 17 carbon atoms. Due to nonpolarity of this chain, there is not strong interaction between water molecules with high polarity and outer surface of the long chain. Therefore, a combination of elevated surface unevenness with low surface free energy acquired by chemisorption of STA have been regarded as two fundamental reasons for WCA increase as well as superhydrophobicity state.

4.4. Corrosion resistance

The polarization curve measurements were carried out to estimate the ability of the superhydrophobic coating to protect the Al substrate from corrosion in NaCl solution (3.5% w/w) using Tafel extrapolation method. The corrosion resistance of different samples can be compared from the corrosion potential (E_{corr}) and the corrosion current density (i_{corr}). The lower i_{corr} and more positive E_{corr} indicate the enhanced corrosion resistance [32–34]. Based on Fig. 9, for B. Al, E_{corr} is −0.758 V and this value shifts positively to −0.718 V and −0.723 V for STA–ZnO–Al–U and STA–ZnO–Al(E)–U, respectively. Also, i_{corr} is about 2.238×10^{-5} A cm^{-2} for B. Al.

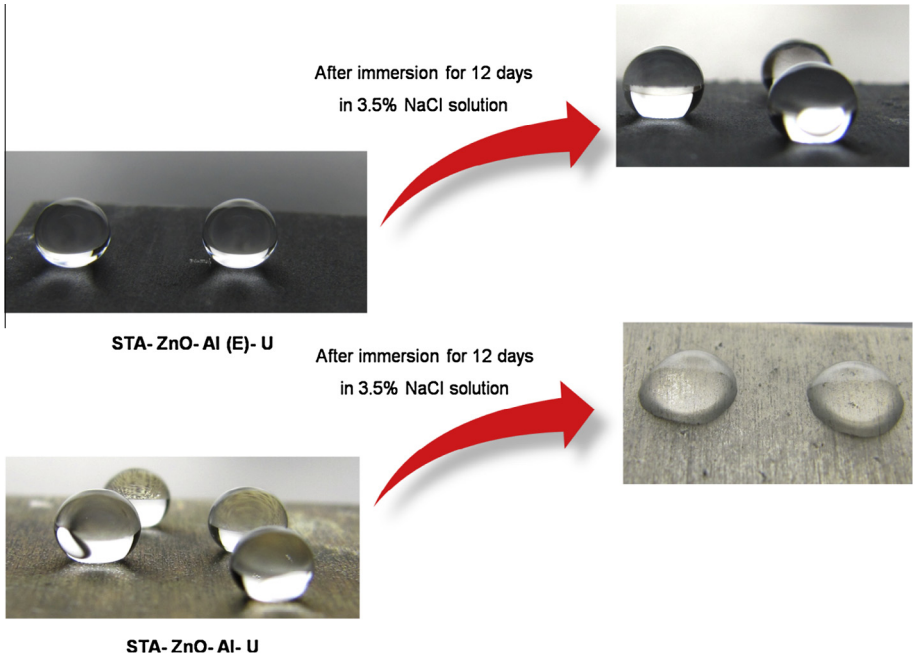

Fig. 11. Water droplet images on M.E.Z. Al and M.Z. Al. US surfaces after long-term stability test in 3.5% NaCl solution for 12 days.

After creation of superhydrophobic property on B. Al, i_{corr} decreased for both superhydrophobic surfaces. But, this decline is more significant for STA–ZnO–Al(E)–U in comparison with STA–ZnO–Al–U. For mentioned surfaces, i_{corr} is 1.250×10^{-6} A cm^{-2} and 1.047×10^{-5} A cm^{-2}, correspondingly.

Overall, for both superhydrophobic surfaces (STA–ZnO–Al–U and STA–ZnO–Al(E)–U), E_{corr} shifts to positive value and i_{corr} decreases in comparison with B. Al. However, the decline of i_{corr} is more considerable for STA–ZnO–Al(E)–U. This means that for STA–ZnO–Al(E)–U surface, corrosion resistance has been improved effectively in comparison with STA–ZnO–Al–U ones.

For more study, the long-term stability of STA–ZnO–Al–U and STA–ZnO–Al(E)–U in NaCl solution (3.5%) has been investigated. The results are demonstrated in Fig. 10. Furthermore, the images of water droplets on mentioned surfaces have been shown after 12 days immersion in 3.5% NaCl solution (Fig. 11). Based on these figures, STA–ZnO–Al(E)–U surface has higher stability than STA–ZnO–Al–U.

Superhydrophobic surfaces have large fraction of trapped air between the grooves, which can reduce the contact area between water and solid surface. Therefore, superhydrophobic surfaces can keep away any species with hydrophilic property. As a result, corrosive Cl^- cannot penetrate into the Al surface and this leads to the enhancement of the corrosion resistance of the superhydrophobic surface (Fig. 9). It is necessary to emphasize that superhydrophobic surfaces with hierarchical structure can maintain more air pocket between surface grooves in comparison with one-scale rough surface. For this reason, the long-term stability of STA–ZnO–Al(E)–U is considerably higher than STA–ZnO–Al–U.

5. Conclusion

Generally, a simple immersion method accompanied with ultrasound was proposed to fabricate desirable roughness on Al through ZnO particle deposition. Modification with STA as a final step can lead to superhydrophobicity of the surface. The results show that sonication is more effective than classic one to fabricate superhydrophobic surfaces. In another way, etching of Al in HCl (10%) for 10 min was carried out before ZnO particle deposition using ultrasound method. After etching, the ZnO particle deposition yields a hierarchical structure with more mechanically stable superhydrophobic property after STA modification. The potentiodynamic measurements demonstrate that the decline of i_{corr} is major for STA–ZnO–Al(E)–U in comparison with STA–ZnO–Al–U. Finally, long-term stability assessment demonstrated that STA–ZnO–Al(E)–U has significant stability versus immersion in NaCl solution up to 12 days.

Appendix A. Supplementary material

Supplementary data associated with this article can be found, in the online version, at http://dx.doi.org/10.1016/j.jcis.2015.10.029.

References

[1] N. Verplanck, Y. Coffinier, V. Thomy, R. Boukherroub, Wettability switching techniques on superhydrophobic surfaces, Nanoscale Res. Lett. 2 (2007) 577–596.
[2] J. Li, X. Liu, Y. Ye, H. Zhou, J. Chen, Fabrication of superhydrophobic CuO surfaces with tunable water adhesion, J. Phys. Chem. C 115 (2011) 4726–4729.
[3] R. Blossey, Self-cleaning surfaces—virtual realities, Nat. Mater. 2 (2003) 301–306.
[4] R. David, A.W. Neumann, Computation of the wetting properties of randomly structured superhydrophobic surfaces, J. Phys. Chem. C 116 (2012) 16601–16608.
[5] X. Gao, L. Jiang, Biophysics: water-repellent legs of water striders, Nature 432 (2004) 36.
[6] Z. She, Q. Li, Z. Wang, L. Li, F. Chen, J. Zhou, Novel method for controllable fabrication of a superhydrophobic CuO surface on AZ91D magnesium alloy, ACS Appl. Mater. Interfaces 4 (2012) 4348–4356.
[7] L. Yao, M. Zheng, L. Ma, W. Li, M. Li, W. Shen, Self-assembly of diverse alumina architectures and their morphology-dependent wettability, Mater. Res. Bull. 46 (2011) 1403–1408.
[8] A.M. Escobar, N. Llorca-Isern, Superhydrophobic coating deposited directly on aluminum, Appl. Surf. Sci. 305 (2014) 774–782.
[9] Y. Zhang, J. Wu, X. Yu, H. Wu, Low-cost one-step fabrication of superhydrophobic surface on Al alloy, Appl. Surf. Sci. 257 (2011) 7928–7931.
[10] Y. Wang, B. Li, T. Liu, C. Xu, Z. Ge, Controllable fabrication of superhydrophobic TiO_2 coating with improved transparency and thermostability, Colloids Surf., A 441 (2014) 298–305.
[11] Q. Wang, B. Zhang, M. Qu, J. Zhang, D. He, Fabrication of superhydrophobic surfaces on engineering material surfaces with stearic acid, Appl. Surf. Sci. 254 (2008) 2009–2012.

[12] D. Nystrom, J. Lindqvist, E. Ostmark, P. Antoni, A. Carlmark, A. Hult, E. Malmstrom, Superhydrophobic and self-cleaning bio-fiber surfaces via ATRP and subsequent postfunctionalization, ACS Appl. Mater. Interfaces 1 (2009) 816–823.
[13] W. Liu, Y. Luo, L. Sun, R. Wu, H. Jiang, Y. Liu, Fabrication of the superhydrophobic surface on aluminum alloy by anodizing and polymeric coating, Appl. Surf. Sci. 264 (2013) 872–878.
[14] S. Ji, P.A. Ramadhianti, T.-B. Nguyen, W.-D. Kim, H. Lim, Simple fabrication approach for superhydrophobic and superoleophobic Al surface, Microelectron. Eng. 111 (2013) 404–408.
[15] Y. Wu, C. Zhang, Analysis of anti-condensation mechanism on superhydrophobic anodic aluminum oxide surface, Appl. Therm. Eng. 58 (2013) 664–669.
[16] Y. Guo, Q. Wang, T. Wang, Facile fabrication of superhydrophobic surface with micro/nanoscale binary structures on aluminum substrate, Appl. Surf. Sci. 257 (2011) 5831–5836.
[17] Z. Darvishi, A. Morsali, Synthesis and characterization of nano-bentonite by sonochemical method, Ultrason. Sonochem. 18 (2011) 238–242.
[18] Z. Sharifalhoseini, M.H. Entezari, The new aspects of the anticorrosive ZnO@SiO_2 core–shell NPs in stabilizing of the electrolytic Ni bath and the Ni coating structure; electrochemical behavior of the resulting nano-composite coatings, J. Colloid Interface Sci. 455 (2015) 110–116.
[19] J. Song, W. Xu, X. Liu, Y. Lu, Z. Wei, L. Wu, Ultrafast fabrication of rough structures required by superhydrophobic surfaces on Al substrates using an immersion method, Chem. Eng. J. 211–212 (2012) 143–152.
[20] Gang Ou, Dongke Li, Wei Pan, Qinghua Zhang, Ben Xu, Lin Gu, Cewen Nan, Hui Wu, Arc-melting to narrow the bandgap of oxide semiconductors, Adv. Mater. 27 (2015) 2589–2594.
[21] K. Murali, P. Thirumoorthy, Characteristics of sol–gel deposited alumina films, J. Alloys Compd. 500 (2010) 93–95.
[22] T. Ivanova, A. Harizanova, T. Koutzarova, B. Vertruyen, Preparation and characterization of ZnO–TiO_2 films obtained by sol–gel method, J. Non-Cryst. Solids 357 (2011) 2840–2845.
[23] S.P. Ansari, F. Mohammad, Studies on nanocomposites of polyaniline and zinc oxide nanoparticles with supporting matrix of polycarbonate, ISRN Mater. Sci. 2012 (2012).
[24] S.P. Ansari, F. Mohammad, Electrical studies on the composite of polyaniline with Zinc oxide nanoparticles, IUP J. Chem. 4 (2010) 7–18.
[25] Y.J. Kwon, K.H. Kim, C.S. Lim, K.B. Shim, Characterization of ZnO nanopowders by the polymerized complex method via an organochemical route, J. Ceram. Process. Res. 3 (2002) 146–149.
[26] R.F. Silva, M.E. Zaniquelli, Morphology of nanometric size particulate aluminium-doped zinc oxide films, Colloids Surf., A 198 (2002) 551–558.
[27] H. Li, J. Wang, H. Liu, C. Yang, H. Xu, X. Li, H. Cui, Sol–gel preparation of transparent zinc oxide films with highly preferential crystal orientation, Vacuum 77 (2004) 57–62.
[28] F. Alvi, M.K. Ram, H. Gomez, R.K. Joshi, A. Kumar, Evaluating the chemio-physio properties of novel zinc oxide–polyaniline nanocomposite polymer films, Polym. J. 42 (2010) 935–940.
[29] D. Steele, Infrared spectroscopy: theory, Handbook of Vibrational Spectroscopy, DOI, 2006.
[30] G. Thirumala Rao, B. Babu, R. Joyce Stella, V. Pushpa Manjari, R.V.S.S.N. Ravikumar, Spectral investigations on undoped and Cu^{2+} doped ZnO–CdS composite nanopowders, Spectrochim. Acta Part A Mol. Biomol. Spectrosc. 139 (2015) 86–93.
[31] S. Wang, J. Shi, C. Liu, C. Xie, C. Wang, Fabrication of a superhydrophobic surface on a wood substrate, Appl. Surf. Sci. 257 (2011) 9362–9365.
[32] D. Lv, J. Ou, M. Xue, F. Wang, Stability and corrosion resistance of superhydrophobic surface on oxidized aluminum in NaCl aqueous solution, Appl. Surf. Sci. 333 (2015) 163–169.
[33] S. Khorsand, K. Raeissi, F. Ashrafizadeh, Corrosion resistance and long-term durability of super-hydrophobic nickel film prepared by electrodeposition process, Appl. Surf. Sci. 305 (2014) 498–505.
[34] L. Feng, H. Zhang, Z. Wang, Y. Liu, Superhydrophobic aluminum alloy surface. Fabrication, structure, and corrosion resistance, Colloids Surf., A 441 (2014) 319–325.